Aortic arch anatomy characterization from MRA: A CNN-based segmentation approach

Mounir Lahlouh, Yasmina Chenoune, Raphaël Blanc, Jérome Szewczyk, Nicolas Passat

AORTIC ARCH ANATOMY CHARACTERIZATION FROM MRA: A CNN-BASED SEGMENTATION APPROACH

Mounir Lahlouh[1,2,3], *Yasmina Chenoune*[2,4], *Raphaël Blanc*[3,5], *Jérôme Szewczyk*[3,6], *Nicolas Passat*[1]

[1] CReSTIC, Université de Reims Champagne Ardenne, Reims, France
[2] ESME Sudria Research Lab, Paris, France
[3] Basecamp Vascular, Paris, France
[4]LISSI, Université Paris-Est, Vitry-sur-Seine, France
[5] Fondation Ophtalmologique de Rothschild, Interventional Neuroradiology Department, Paris, France
[6] ISIR, Sorbonne Université, Paris, France

ABSTRACT

Neurovascular pathologies are often treated with the help of imaging to guide catheters inside arteries. However, positioning a microcatheter into the aortic arch and threading it through blood vessels for embolization, mechanical thrombectomy or stenting is a challenging task. Indeed, adverse aortic arch anatomies are frequently encountered, especially when the aortic arch is dilated, or the supra-aortic branches are elongated and tortuous. In this article, we propose a pipeline using convolutional neural networks for the segmentation of the aortic arch from magnetic resonance images for further anatomy classification purpose. This pipeline is composed of two successive modules, dedicated to the localization and the accurate segmentation of the aortic arch and the origin of supra-aortic branches, respectively. These segmentations are then used to generate 3D models from which the anatomy and the type of the aortic arches can be characterized. A quantitative evaluation of this approach, carried out on various U-Net architectures and different optimizers, leads to satisfactory segmentation results, then allowing a reliable characterization.

Index Terms— Aortic arch, segmentation, characterization, U-Net, magnetic resonance angiography, endovascular therapy.

1. INTRODUCTION

Neurovascular diseases are mainly treated by endovascular procedures such as embolization, mechanical thrombectomy or stenting. However, the tools used by physicians are not always maneuverable and intuitive. Thus, to choose the catheter best fitting the patient's morphology and to anticipate the neuroradiologist gesture, an anatomical study of the vessels is essential, especially at the level of the aortic arch, due to its interpatient anatomical variability.

The aortic arch is a complex structure, which has been the subject of several studies aiming to characterize and classify its anatomy according to different criteria. To this end, Madhwal's classification [1], according to [2], appears to be easier to reproduce and provides relevant clinical outcomes. Besides, it is less frequently influenced by pathological derangements of the aortic wall such as aneurysms compared to Casserly's classification [3]. In Madhwal's classification (Fig. 1), the comparison between the diameter of the left common carotid artery (CCA) and the vertical distance from the top of the aortic arch to the origin of the brachiocephalic branch (BCA) determines the arch type. This leads to the definition of three types (I, II and III) that constitute an anatomical standard according to many contemporary guidelines on thoracic aortic repairing [4, 5].

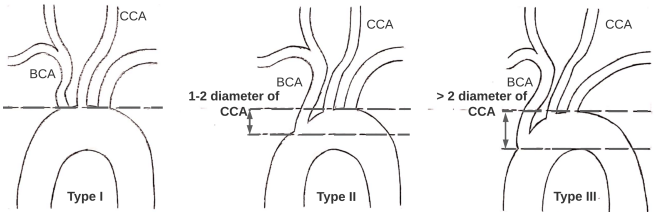

Fig. 1. Aortic arch anatomy classification [1]. Type I: the distance from the top of the aortic arch to the origin of the BCA is lower than CCA diameter. Type II: the distance is between 1 and 2 times CCA diameter. Type III: the distance is more than 2 times CCA diameter.

In Madhwal's classification, each type of arch has its own anatomical and biomechanical characteristics that have clinical implications in the prevalence of neurovascular diseases. For instance, the type III aortic arch is characterized by an increase in angulation and tortuosity of supra-aortic branches. As a consequence, it was shown that type III arch is strongly correlated with the risk of type B aortic dissection and type B intramural hematoma [6].

The arch anatomy plays a major role in predicting the success of endovascular procedures but the studies on the impact of aortic arch types on procedural complexity and outcomes are recent. For example, in carotid artery stenting (CAS), catheter manipulation time (CMT) is significantly influenced by the aortic arch type. Therefore, patients with type III arch have a longer CMT compared to type I or type II [7] which increases the risk for adverse outcome. Type III arches are also associated with more difficulties and complications in CAS procedures [8]. Identifying the type of aortic arch before endovascular procedures is then crucial since it provides information on the complexity of navigation to the pathological area, and can help physicians to better plan procedures and choose the most appropriate catheter.

Several works have been proposed for the segmentation of the aorta in which different approaches were used to better capture its angioarchitecture. An atlas-based method combined with registration technique was applied for aorta segmentation in computed tomography (CT) scans [9]. In [10] a multi-atlas approach was considered to localize abdominal organs including the abdominal aorta in CT scans before feeding a 3D convolutional neural network (CNN)

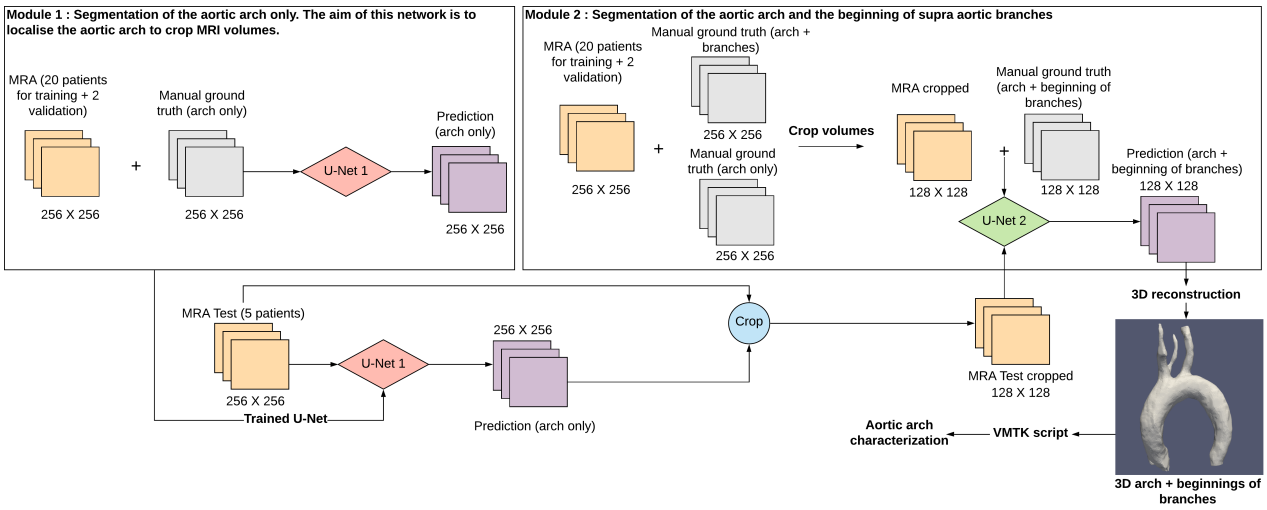

Fig. 2. The proposed CNN-based pipeline consists of two modules: the first for localizing, recentering, and cropping volumes around the aortic arch (U-Net 1), the second for the segmentation of the arch and the beginnings of supra-aortic branches (U-Net 2).

for organs segmentation. Multi-view 2D CNN approaches were also applied for multipart segmentation of the aorta. An automatic segmentation of the ascending aorta, the aortic arch, and the descending aorta in low-dose chest CT scans was proposed using dilated CNN [11]. It aggregates the classification of voxels in axial, sagittal, and coronal CT slices. The same idea has been used in [12] for the segmentation of the aortic lumen from the ascending aorta to the iliac arteries. In this study, a CNN-based pipeline localizes the aorta in CT scans before carrying out its segmentation. The paradigm of combining localization with segmentation has also been used in [13] for aorta segmentation from CT cardiac angiography using U-Net architectures. In the context of detection and diagnosis of abdominal aortic aneurysm, in [14] a classifier using CNN on aorta CT angiography patches aims to detect the aorta, before carrying out diameter estimation. In [15], a CT angiography multi-stage segmentation pipeline of type B aortic dissection was proposed. In this study, two cascaded CNNs were used, the first for the segmentation of aortic branches and the second for the segmentation of the true and false lumen of the type B aortic dissection.

To the best of our knowledge and despite the importance of aortic arch anatomical typology, none of the approaches involving deep neural architectures in aorta segmentation procedures have proposed an automated pipeline aiming to characterize the aortic arch in its three categories. In addition, the segmentation methods proposed in the literature only deal with CT images, which are easier to analyse than Magnetic Resonance Angiographic (MRA) images. However, MRAs are important in our context, since many French healthcare institutions treat patients in the acute phase of stroke with MRA modality. In this article, we tackle this issue, by proposing a CNN-based pipeline composed of two modules relying on U-Net models [16]: one for localizing and cropping MRA volumes around the aortic arch and the origins of the supra-aortic branches, the other for the vascular structures segmentation from the cropped area. Different U-Net architectures are investigated and we also assess the performance of a new adaptive optimizer, namely AdaBelief [17], versus other standard optimizers.

This article is organized as follows. The proposed CNN pipeline and its settings are described in Sec. 2. The results are presented and discussed in Sec. 3. Conclusions and perspectives are given in Sec. 4.

2. MATERIAL AND METHOD

2.1. Data acquisition and preprocessing

A dataset[1] of 27 MRA volumes was collected. They were obtained from patients between 31 and 95 years old (avg. 72 years, 59%/41% of male/female).

Patients underwent 3T MR exams on Philips imaging system (Ingenia 3T, Best, The Netherlands) using a 16 channels head coil. All examinations included a contrast enhanced MRA of aortic arch, supra-aortic trunks and intracranial vessels using the following parameters: coronal plane covering: 250 slices; active TR/TE $= 5.5/2.2$ ms; flip angle $= 27°$; number of excitations $= 1$; acquisition bandwidth = 476.7 Hz; FOV $= 380 \times 321$; voxel size = $0.5 \times 0.5 \times 1.0$ mm (with further interpolation, see below). The imaging time was 69 sec. Bolus track injection technique was used to time the start of data acquisition.

Aortic arch types of these volumes were assigned by experienced neuroradiologists. Types II or III were observed in 18.5% of patients, respectively compared to 63% of type I.

The whole dataset is not fully homogeneous. Most of the MRA volumes have a resolution of $0.495 \times 0.495 \times 0.500$ mm after interpolation. This can be problematic for automatic analysis using deep learning architectures. To deal with this issue, we resampled the whole dataset using spline interpolation to an isotropic resolution of $1 \times 1 \times 1$ mm, leading to coronal slices of size 256×256. MRA volumes intensities were also normalized (mean and standard deviation values) in order to provide comparable data.

2.2. Data labeling and augmentation

The aortic arch and supra-aortic branches in MRA volumes were 3D modeled with Materialise Mimics software[2]. The generated STL

[1]This dataset is private. It was provided by the Department of Neuroradiology of the Adolphe de Rothschild Foundation Hospital, Paris, France.

[2]https://www.materialise.com/medical/mimics-innovation-suite/mimics

meshes, were manually corrected and validated by neuroradiologists. Coronal slices were then extracted from these labeled data and automatically overlapped on the patients' DICOM volumes using 3D Slicer software[3]. Two sets of ground-truth binary masks were then created: one for the aortic arch only and another for the whole aorta (aortic arch and supra-aortic branches).

The two sets of ground-truths and the MRA volumes were organized into 2D slices (6 849 images) to feed the CNN-based pipeline. Twenty patients were used for training the CNNs, two for the validation set and five for the test set.

To avoid overfitting and improve generalization, we augmented our dataset using random operations (rotations, translations and rescalings) during the training and validation phases in order to enlarge the set of examples handled by the CNNs.

2.3. CNN-based segmentation pipeline

The proposed pipeline consists of two modules (Fig. 2) based on U-Net-like architectures that have proven their success in medical image segmentation where the amount of data is small. The first module aims at localizing the aortic arch in the initial (256×256) images, in order to determine cropped (128×128) images focusing on it. To reach that goal, we rely on the ground-truths of the only aortic arches associated with patients' MRA slices to feed a standard U-Net. As this first network carries out a localization task via a rough segmentation of the aortic arch; this segmentation does not need to be fully accurate. The segmentation output is post-processed (smoothing, hole filling, area filtering), and a cuboid is defined as the bounding box of the resulting segmentation. This cuboid is dilated by 25 pixels in the coronal slices to generate a volume centered on the aortic arch. This volume then allows to define cropped coronal slices of dimension 128×128 that can be involved in the second segmentation module.

This second module aims to carry out a fine segmentation of the cropped images. To reach that goal, we also use the second ground-truth that contains the entire aorta (arch plus supra-aortic branches). Both ground-truths and the cropped 128×128 MRA slices are used to feed a second U-Net-like architecture for the segmentation of the aortic arch and the beginnings of supra-aortic branches. By contrast with the first module, where a standard U-Net architecture was sufficient to obtain a segmentation used for localization purpose, in this second module, the segmentation needs to be fully accurate. As a consequence, various architectures building upon the U-Net paradigm can be considered (see Sec. 3).

To summarize, each new patient goes through the U-Net localization network to have the volumes of interest containing only the arches and the beginnings of supra-aortic branches. Then, these volumes of interest pass through the U-Net segmentation module in order to obtain a binary segmentation. More precisely, an STL mesh is obtained by stacking the 2D segmented slices. These 3D models are post-processed (smoothing, hole filling, removing isolated voxels). They constitute the input for a further geometric characterization of aortic arches developed under the Vascular Modeling Toolkit (VMTK)[4]. In particular, centerlines, takeoff angles and aortic arch type can be easily extracted from such 3D models.

2.4. Experimental settings

Our experiments were performed on an NVIDIA GeForce RTX 3090 (24 GB) graphic card with CUDA compute capability (V11.3), under Windows 10 operating system. The CNN-based pipeline was developed using Python and the deep learning models were implemented in Keras based on Tensorflow GPU support[5]. The evaluation of the models was done by calculating the following metrics: Dice Similarity Coefficient (DSC), Jaccard coefficient (IOU), precision (Prec.), and recall (Rec.).

Table 1. Segmentation results of the first module (localization, cropping) with different optimizers (values given in %).

Optimizer	Metrics	Train	Validation	Test
SGD	DSC	90.02	62.74	81.51
	IOU	84.93	53.63	75.93
	Prec.	96.18	62.91	82.96
	Rec.	83.37	59.71	88.59
Adam	DSC	97.92	87.48	88.11
	IOU	96.73	81.94	83.79
	Prec.	98.54	87.56	**94.58**
	Rec.	97.32	88.93	88.07
AdaBelief	DSC	97.45	86.69	**89.65**
	IOU	96.12	80.98	**85.75**
	Prec.	98.45	84.49	93.75
	Rec.	97.16	87.99	**91.08**

To train the models, different optimizers were used. We assessed the performance of the new AdaBelief optimizer [17] versus Adam [18] and the Stochastic Descent Gradient (SGD) [19]. A learning rate of 10^{-4} decreasing by a factor of 0.9 with patience value set to 5 epochs if no improvement was noticed on DSC of the validation set. A batch size of 8 and 32 slices randomly sampled was provided for the localization and the segmentation CNNs, respectively. The slices in each batch for each iteration were augmented on the fly for the training and validation phases. The training process was stopped after 20 epochs if no improvement was noticed on DSC of the validation set.

The dataset suffers from the usual class imbalance problem. This can significantly alter the optimization if the considered loss function does not take into account this lack of equilibrium. For these reasons, we focused on the Focal Tversky (FT) loss [20] and its combination with binary cross-entropy (CE) for the segmentation of small structures and imbalanced datasets. We have:

$$\text{FT} = \sum_c \Big(1 - \frac{\sum_i p_{ic} g_{ic} + \varepsilon}{\sum_i p_{ic} g_{ic} + \alpha \sum_i p_{i\bar{c}} g_{ic} + \beta \sum_i p_{ic} g_{i\bar{c}} + \varepsilon}\Big)^{1/\gamma}$$

with c the two classes; i the pixels; $0 < \varepsilon \ll 1$; $g_{ic} = 1$ (resp. 0) if $i \in c$ (resp. $\notin c$); $p_{ic} \in [0, 1]$ the prediction of $i \in c$. The α and β parameters handle the trade-off between false positives and false negatives; $\gamma \in [1, 3]$ is the focal parameter. Based on our experiments, we set $\alpha = 0.4$, $\beta = 0.6$, $\gamma = 4/3$.

Since the aim of the first CNN in the pipeline is to localize the aortic arches, a precise segmentation is not required. Thus, we only used the standard U-Net model from [16]. By contrast, the second CNN model has to carry out an accurate segmentation of the aortic arches and the beginnings of supra-aortic branches. In this context, different variants of U-Net architectures were investigated to evaluate their effectiveness for this task. In particular, we considered the Attention U-Net [21] and Inception U-Net [22] architectures, in addition to the standard U-Net.

[3] https://www.slicer.org

[4] http://www.vmtk.org

[5] All results and developments described in this article are the property of Basecamp Vascular and fall within the scope of its research and development needs.

Table 2. Segmentation results of the second module (fine segmentation) with different U-Net-like architectures and optimizers.

Model	Optimizer	Train (%)				Validation (%)				Test (%)			
		DSC	IOU	Prec.	Rec.	DSC	IOU	Prec.	Rec.	DSC	IOU	Prec.	Rec.
U-Net	SGD	31.50	21.26	53.74	39.86	35.46	23.33	39.83	43.86	34.96	25.00	27.85	**97.21**
	Adam	94.21	91.55	96.76	94.95	75.66	67.96	82.59	83.03	82.95	75.96	73.48	94.65
	AdaBelief	95.40	92.86	97.06	95.29	77.15	68.80	84.10	72.99	85.15	79.00	78.77	91.93
Attent. U-Net	SGD	61.80	56.02	90.73	83.61	41.16	34.79	79.49	58.05	80.14	72.29	76.84	85.73
	Adam	95.27	92.79	97.33	95.35	76.82	67.70	83.00	74.51	83.78	77.15	79.24	90.69
	AdaBelief	94.78	92.12	97.02	94.96	78.47	70.03	84.73	76.09	84.05	77.33	79.24	91.05
Incept. U-Net	SGD	76.54	73.37	96.34	93.72	56.63	48.66	81.34	71.43	79.25	71.33	71.09	92.56
	Adam	87.03	84.65	97.28	95.74	77.80	70.46	87.87	81.31	87.73	82.11	82.84	93.86
	AdaBelief	93.28	91.21	97.68	96.39	80.91	73.59	88.50	79.98	**88.07**	**82.56**	**84.10**	93.80

3. RESULTS AND DISCUSSION

Experiments for both localization and segmentation modules were carried out and the different models were run during 150 epochs. We report the mean of each evaluation metric (DSC, IOU, Prec. and Rec.) for 3 runs with random initialization for each optimizer.

Regarding the first module (localization), the standard U-Net model [16] with different optimizers was trained. The obtained results are summarized in Tab. 1. The best scores for the test set were achieved using AdaBelief and Adam optimizers with a slight advantage to the first one. In particular, AdaBelief achieves a DSC of 89.65% and an IOU of 85.75% with respect to the ground-truth provided by experts. We also notice a reduction in the difference between precision and recall when using AdaBelief optimizer ($|\text{Prec.}-\text{Rec.}| = 2.67\%$) compared to SGD and Adam.

Regarding the second module (segmentation), that requires a higher accuracy, we tested 3 architectures: U-Net [16], Attention U-Net [21] and Inception U-Net [22] with the same optimizers as the previous experiment. Results are summarized in Tab 2. The training of the Inception U-Net with the AdaBelief optimizer achieved the best DSC (88.07%) and IOU (82.56%), and also the best precision. This combination also minimizes the gap between precision and recall on the test set. Attention U-Net showed promising results with a DSC of 84.05%. The use of attention gates, that perform features selectivity, and inception blocks, that increase the depth of the U-Net network, seems to improve generalization ability.

In [17] it is claimed that AdaBelief achieves three goals: generalization, fast convergence, and training stability. In our segmentation problem, AdaBelief actually generalizes better than the other tested optimizers, whatever the architecture used. The results obtained with Inception U-Net + AdaBelief are exemplified in Fig. 3.

The predicted binary masks generated as output of our pipeline were used for the reconstruction of 3D models as illustrated in Fig. 4. These 3D models contain both the aortic arch and the beginnings of supra-aortic branches (BCA and CCA arteries). From such model, Madhwal's classification rules can be easily applied to determine the arch type. Using the VMTK library, the BCA and CCA arteries are determined so that the vertical distance from the top of the aortic arch to the origin of the brachiocephalic branch (BCA) can be compared to the diameter of the left common carotid artery (CCA). Other characteristics (bifurcation angles, centerlines) can be also extracted.

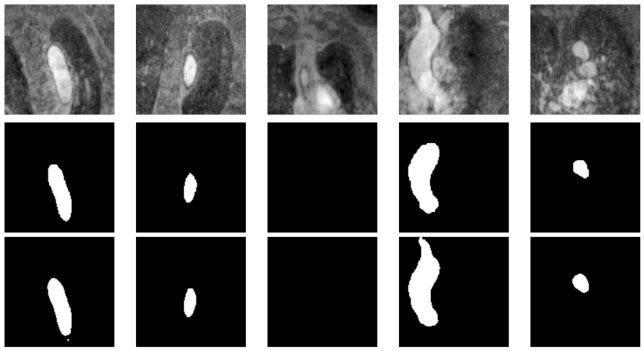

Fig. 3. First row: MRA slices (coronal view). Second row: ground-truth segmentation. Third row: segmentation results obtained with our pipeline (Inception U-Net + AdaBelief).

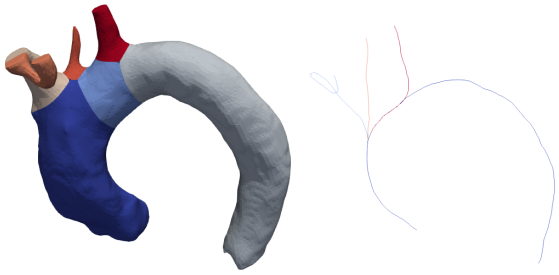

Fig. 4. 3D model (left) and centerlines (right) of an aortic arch with the origins of supra-aortic branches generated from the proposed CNN-based pipeline.

4. CONCLUSION AND PERSPECTIVES

In order to automatically characterize the aortic arch from MRA volumes, we proposed a CNN-based pipeline composed of two modules: localization and segmentation of the aortic arches and the origins of supra-aortic branches. The best results were achieved with the AdaBelief optimizer using the Inception U-Net architecture. The binary masks predicted are quite similar to the ground-truth validated by neuroradiologists. These binary masks are then used to construct 3D models of the aortic arch that can be easily involved for characterization purpose, which is essential in interventional neuroradiology.

This work could be improved by increasing our dataset size, enhancing the tested models or investigating variants like UNet++ or TransUNet for a better generalization. This approach could also be extended beyond the aortic arch characterization. Indeed, this pipeline could be improved to provide a complete segmentation of the supra-aortic branches so that other factors such as tortuosity and angulations of supra-aortic branches could be calculated.

5. COMPLIANCE WITH ETHICAL STANDARDS

This research study was conducted retrospectively using human patients' data. An oral and written information about image post-processing was delivered. The study was approved by the Institutional Ethical Committee in accordance with the 1964 Helsinki declaration and its later amendments. Written consent was waived.

6. ACKNOWLEDGMENTS

The authors acknowledge the *Fondation Ophtalmologique Adolphe de Rothschild* for the clinical MR images used in this research.

This work was financially supported by Basecamp Vascular, a French company that develops mechatronic active catheters dedicated to endovascular navigation, and by the French *Association Nationale de la Recherche et de la Technologie* (ANRT) (grant 2020/0638).

M. Lahlouh is funded by Basecamp Vascular. R. Blanc is a founder and director of Basecamp Vascular. J. Szewczyk is a founder of Basecamp Vascular.

7. REFERENCES

[1] S. Madhwal, V. Rajagopal, D. L. Bhatt, C. T. Bajzer, P. Whitlow, and S. R. Kapadia, "Predictors of difficult carotid stenting as determined by aortic arch angiography," *J Invasive Cardiol*, vol. 20, pp. 200–204, 2008.

[2] M. M. Marrocco-Trischitta and M. Glauber, "Implications of different definitions for aortic arch classification provided by contemporary guidelines on thoracic aortic repair," *Interact Cardiov Th*, vol. 32, pp. 950–952, 2021.

[3] I. P. Casserly, R. Sachar, and J. S. Yadav, *Manual of Peripheral Vascular Intervention*, Lippincott Williams & Wilkins, 2005.

[4] B. Rylski, D. Pacini, F. Beyersdorf, E. Quintana, T. Schachner, K. Tsagakis, S. Ronchey, A. Durko, R. De Paulis, M. Siepe, E. E. Roselli, T. Carrel, M. Czerny, F. S. Schoenhoff, and EACTS Vascular Domain, EJCTS and ICVTS Editorial Committees, "Standards of reporting in open and endovascular aortic surgery (STORAGE guidelines)," *Eur J Cardio-Thorac*, vol. 56, pp. 10–20, 2019.

[5] G. R. Upchurch Jr, G. A. Escobar, A. Azizzadeh, A. W. Beck, M. F. Conrad, J. S. Matsumura, M. H. Murad, R. J. Perry, M. J. Singh, R. K. Veeraswamy, and G. J. Wang, "Society for Vascular Surgery clinical practice guidelines of thoracic endovascular aortic repair for descending thoracic aortic aneurysms," *J Vasc Surg*, vol. 73, pp. 55S–83S, 2021.

[6] M. M. Marrocco-Trischitta, B. Rylski, F. Schofer, F. Secchi, G. Piffaretti, H. De Beaufort, V. Belvroy, J. Bismuth, M. Czerny, and S. Trimarchi, "Prevalence of type III arch configuration in patients with type B aortic dissection," *Eur J Cardio-Thorac*, vol. 56, pp. 1075–1080, 2019.

[7] F. Burzotta, R. Nerla, G. Pirozzolo, C. Aurigemma, G. Niccoli, A. M. Leone, S. Saffioti, F. Crea, and C. Trani, "Clinical and procedural impact of aortic arch anatomic variants in carotid stenting procedures," *Catheter Cardio Inte*, vol. 86, pp. 480–489, 2015.

[8] S. Shen, X. Jiang, H. Dong, M. Peng, Z. Wang, W. Che, Y. Zou, and Y. Yang, "Effect of aortic arch type on technical indicators in patients undergoing carotid artery stenting," *J Int Med Res*, vol. 47, pp. 682–688, 2019.

[9] I. Isgum, M. Staring, A. Rutten, M. Prokop, M. A. Viergever, and B. Van Ginneken, "Multi-atlas-based segmentation with local decision fusion–Application to cardiac and aortic segmentation in CT scans," *IEEE T Med Imaging*, vol. 28, pp. 1000–1010, 2009.

[10] M. Larsson, Y. Zhang, and F. Kahl, "Deepseg: Abdominal organ segmentation using deep convolutional neural networks," in *Swedish Symposium on Image Analysis*, 2016.

[11] J. M. Noothout, B. D. De Vos, J. M. Wolterink, and I. Isgum, "Automatic segmentation of thoracic aorta segments in low-dose chest CT," in *Medical Imaging: Image Processing*, 2018, p. 105741S.

[12] A. Fantazzini, M. Esposito, A. Finotello, F. Auricchio, B. Pane, C. Basso, G. Spinella, and M. Conti, "3D automatic segmentation of aortic computed tomography angiography combining multi-view 2D convolutional neural networks," *Cardiovasc Eng Techn*, vol. 11, pp. 576–586, 2020.

[13] S. R. Ravichandran, B. Nataraj, S. Huang, Z. Qin, Z. Lu, A. Katsuki, W. Huang, and Z. Zeng, "3D inception U-Net for aorta segmentation using computed tomography cardiac angiography," in *BHI*, 2019, pp. 1–4.

[14] S. Mohammadi, M. Mohammadi, V. Dehlaghi, and A. Ahmadi, "Automatic segmentation, detection, and diagnosis of abdominal aortic aneurysm (AAA) using convolutional neural networks and Hough circles algorithm," *Cardiovasc Eng Techn*, vol. 10, pp. 490–499, 2019.

[15] D. Chen, X. Zhang, Y. Mei, F. Liao, H. Xu, Z. Li, Q. Xiao, W. Guo, H. Zhang, T. Yan, J. Xiong, and Y. Ventikos, "Multi-stage learning for segmentation of aortic dissections using a prior aortic anatomy simplification," *Med Image Anal*, vol. 69, pp. 101931, 2021.

[16] O. Ronneberger, P. Fischer, and T. Brox, "U-Net: Convolutional networks for biomedical image segmentation," in *MICCAI*, 2015, pp. 234–241.

[17] J. Zhuang, T. Tang, Y. Ding, S. C. Tatikonda, N. C. Dvornek, X. Papademetris, and J. S. Duncan, "AdaBelief optimizer: Adapting stepsizes by the belief in observed gradients," in *NeurIPS*, 2020.

[18] D. P. Kingman and J. Ba, "Adam: A method for stochastic optimization," in *ICLR*, 2015.

[19] H. Robbins and S. Monro, "A stochastic approximation method," *Ann Math Stat*, vol. 22, pp. 400–407, 1951.

[20] N. Abraham and N. M. Khan, "A novel focal Tversky loss function with improved attention U-Net for lesion segmentation," in *ISBI*, 2019, pp. 683–687.

[21] O. Oktay, J. Schlemper, L. L. Folgoc, M. Lee, M. Heinrich, K. Misawa, K. Mori, S. McDonagh, N. Y. Hammerla, B. Kainz, B. Glocker, and D. Rueckert, "Attention U-Net: Learning where to look for the pancreas," in *MIDL*, 2018.

[22] I. Delibasoglu and M. Cetin, "Improved U-Nets with inception blocks for building detection," *J Appl Remote Sens*, vol. 14, pp. 044512, 2020.